Crystal-field effects and the magnetic properties of rare-earth rhodium borides

B. D. Dunlap, L. N. Hall, F. Behroozi, and G. W. Crabtree
Materials Science and Technology Division, Argonne National Laboratory, Argonne, Illinois 60439

D. G. Niarchos
Department of Physics, Illinois Institute of Technology, Chicago, Illinois 60616
(Received 19 December 1983)

The magnetic properties of the $R\mathrm{Rh_4B_4}$ (R represents rare-earth metal) compounds are discussed in terms of a combined crystalline-electric-field and molecular-field approach. Magnetization data taken on single-crystal $\mathrm{ErRh_4B_4}$ in five orientations are used to obtain the crystal-field and molecular-field coefficients, resulting in a complete analysis for the paramagnetic properties of this compound. The crystal-field parameters are additionally used to discuss all previously published magnetic data for polycrystalline $R\mathrm{Rh_4B_4}$ compounds. For these highly anisotropic materials, the effect of preferential crystallite orientation on the observed data is pointed out. Consideration of the variation of the magnetic transition temperature T_m between different constituent rare earths has verified a previous conclusion that the crystal field has a pronounced effect on T_m, but this alone does not fully explain the observations.

I. INTRODUCTION

Since the original observation of reentrant superconductivity, great effort has been devoted to measurements of the physical properties of $\mathrm{ErRh_4B_4}$ and the isostructural compounds containing other rare earths. In particular, a great deal of magnetic data became available as details of the ways in which superconductivity and magnetism could coexist began to be worked out. Such studies revealed a number of very interesting features, such as extremely strong magnetic anisotropies, surprisingly simple mean-field behavior for some ferromagnetic compounds, Curie-law susceptibilities in apparent conflict with the strong crystal-field effects implied by the other data, an unusual variation of the magnetic transition temperature as the rare-earth atom was changed, etc.[1]

It was recognized early that crystalline-electric-field (CEF) effects were very important in determining the properties of these materials. This was seen most clearly by the observation of Schottky anomalies in specific-heat data, and was believed to play a primary role in determining the magnetic properties. Recently, the parameters of the crystal-field Hamiltonian have been evaluated[2] for $\mathrm{ErRh_4B_4}$. Extrapolated to other members of the series, those parameters have been used for a general description of several experimental observations, and for a description of the Schottky specific-heat results.[3] In the following we will present more extensive single-crystal magnetization measurements in $\mathrm{ErRh_4B_4}$. These will be analyzed in a combined crystal-field and molecular-field approach to provide improved crystal-field parameters. The parameters, so obtained, will then be used in a detailed discussion of the effect of CEF interactions on magnetic properties of other $R\mathrm{Rh_4B_4}$ (R represents rare-earth metal) compounds, including a quantitative comparison with the available experimental results.

II. SINGLE-CRYSTAL $\mathrm{ErRh_4B_4}$ MAGNETIZATION DATA AND ANALYSIS

Previous work on single-crystal $\mathrm{ErRh_4B_4}$ has shown the presence of extremely large magnetic anisotropies, with the magnetization along the tetragonal c axis being about 1 order of magnitude smaller than that along the a axis. Anisotropic behavior was also observed in the paramagnetic susceptibility.[4] Based on previous CEF parameters, a magnetic anisotropy in the basal plane was predicted and this was subsequently verified.[5] In the following, we will provide an analysis of these magnetic observations in terms of a combined crystal-field and molecular-field approach.

In the paramagnetic state, the magnetic properties of the material are determined by crystal-field plus Zeeman-interaction terms:

$$\mathcal{H}=\mathcal{H}_{\mathrm{CEF}}-g_J\mu_B\vec{\mathrm{J}}\cdot\vec{\mathrm{H}}\ . \tag{1}$$

The crystal-field Hamiltonian appropriate for the $\bar{4}2m$ symmetry of the rare-earth ions in the $R\mathrm{Rh_4B_4}$ system is

$$\mathcal{H}_{\mathrm{CEF}}=B_2^0O_2^0+B_4^0O_4^0+B_4^4O_4^4+B_6^0O_6^0+B_6^4O_6^4\ , \tag{2}$$

where O_n^m are Stevens operators and B_n^m are constants which must be determined empirically. The magnetic field appearing in the Zeeman term has contributions due to the applied field, the demagnetizing field, the Lorentz field, and the exchange field:

$$H=H_a+H_{\mathrm{demag}}+H_L+H_{\mathrm{ex}}\ . \tag{3}$$

Within usual approximations, all of the last three terms in Eq. (3) are proportional to the magnetization, so we write

$$H=H_a+(\lambda_{\mathrm{demag}}+\lambda_L+\lambda_{\mathrm{ex}})M\equiv H_a+\lambda M\ . \tag{4}$$

For a spherical single crystal, $H_{\mathrm{demag}}=-4\pi/3M$. In a

normal classical calculation of the Lorentz field with a spherical cavity, one obtains $H_L=(4\pi/3)M$, so that the effective field in Eq. (4) consists of the applied field plus the exchange field. However, in noncubic materials the degree to which the demagnetizing fields and the Lorentz fields exactly cancel is not known, and one may additionally expect the Lorentz field to be anisotropic. This problem may not be serious in cases where the magnetic transition temperature is such that $\lambda_{ex}\gg\lambda_{demag},\lambda_L$. However, that is not the case for these materials. We therefore will treat the constant λ as an empirical, temperature-independent parameter which may be anisotropic.

Magnetization data have been obtained in fields up to 2 T for orientations of the single crystal having H_a along the c axis, and in the basal plane at angles of 0°, 17.5°, 27°, and 45° relative to the crystallographic a axis. Susceptibility data were also obtained along the c axis and the a axis in applied fields of 1 T, which is above the superconducting critical field for this material. The field- and temperature-dependent magnetization for the four orientations in the basal plane, the susceptibility along the c axis, and previous data[3] for the Schottky anomaly due to crystal-field levels in the specific heat of $Y_{0.9}Er_{0.1}Rh_4B_4$ were combined simultaneously into a least-squares fitting program. This program calculated the physical parameters under the influence of Eqs. (1)–(4), varying the five crystal-field parameters and the values of λ in the c and a directions. The previously obtained CEF parameters were used as a starting point for the fit, and initial values for λ_a and λ_c were estimated from the magnetic transition temperature of $\sim$1 K. The results of this analysis are compared to the magnetization, susceptibility, and specific-heat data in Figs. 1–3, respectively. In all cases, one sees that the fit is excellent, with the exception of the magnetization data at 2 K, which may indicate short-range ordering effects occurring near the magnetic temperature.

Values of the CEF parameters obtained in the above way are given in Table I. These differ from the previous results primarily in a decrease of B_2^0 by about 30%, and a substantial change in both the signs and magnitudes of the sixth-order parameters. These changes do not significantly alter the calculated properties of the $R\mathrm{Rh}_4\mathrm{B}_4$ compounds from those reported previously,[2] with the exception that the discrepancy between calculation and experiment for the Schottky anomaly in $\mathrm{TbRh}_4\mathrm{B}_4$ is now substantially removed. Therefore, we believe these to represent a real improvement in the CEF parameters. The fits also give the values $\lambda_a=0.0385$ emu/mol$=0.215$ kG/μ_B and $\lambda_c=-0.432$ emu/mol$=-2.41$ kG/μ_B. The value of λ_a is roughly half the value of λ_{ex} expected from the observed susceptibility and magnetic transition temperature. The value of λ_c, being much larger and reversed in sign, is not understood at this point.

The CEF coefficients B_n^m are often written in the form

$$B_n^m=\alpha_n\langle r^n\rangle A_n^m\,, \tag{5}$$

where the $\langle r^n\rangle$ are radial integrals over the $4f$ electrons and the α_n are Stevens factors which are known for any particular ionic configurations. Assuming that the A_n^m are independent of the particular rare-earth ion in an iso-

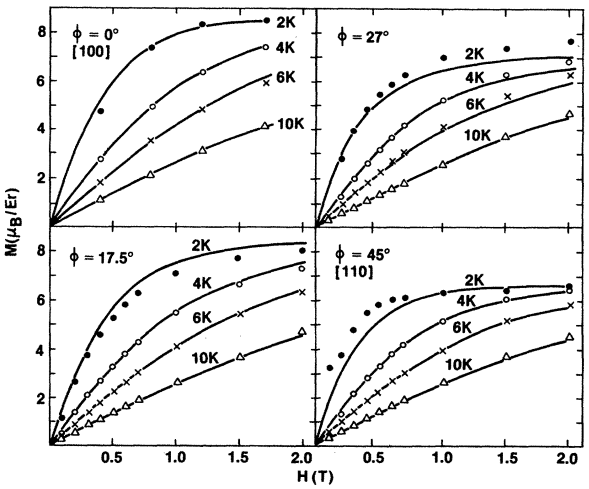

FIG. 2. Solid points give measured magnetization at the indicated orientations relative to the a axis in single crystal $\mathrm{ErRh}_4\mathrm{B}_4$. Solid lines are calculated as described in the text.

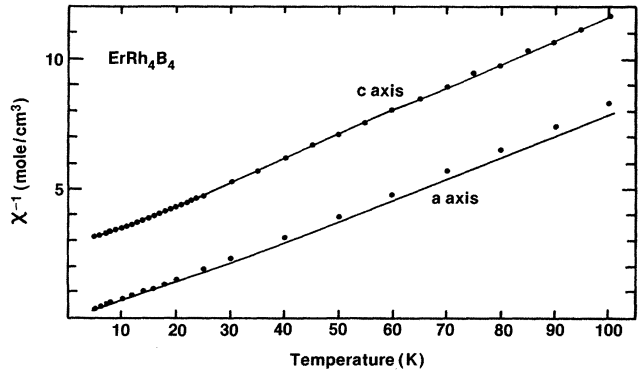

FIG. 1. Solid points give measured susceptibilities $\chi=M/H$ measured at $H=10$ kG along the c and a axes in single-crystal $\mathrm{ErRh}_4\mathrm{B}_4$. Solid lines are calculated as described in the text.

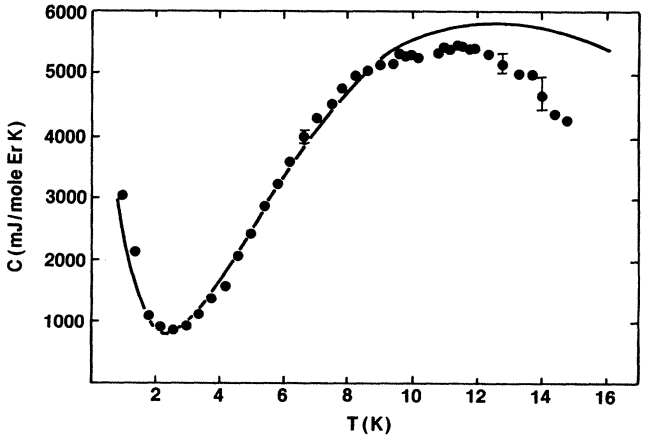

FIG. 3. Measured and calculated magnetic specific heat for $Y_{0.9}Er_{0.1}Rh_4B_4$. Data are from Ref. 3.

TABLE I. CEF parameters for $R\mathrm{Rh_4B_4}$ compounds obtained by scaling according to Eq. (2) from the values obtained for $\mathrm{ErRh_4B_4}$. Values for the various constants in Eq. (5) are summarized in Ref. 19.

R	B_2^0 (K)	B_4^0 (10^{-3} K)	B_4^4 (10^{-3} K)	B_6^0 (10^{-7} K)	B_6^4 (10^{-5} K)
Dy	−1.85	−2.45	9.69	−4.08	3.68
Ho	−0.49	−1.27	5.03	4.49	−4.06
Er	0.53	1.56	−6.19	−6.36	5.74
Tm	2.05	5.44	−21.54	8.61	−7.77

structural series of compunds, and that the radial integrals can be obtained from atomic calculations, the CEF parameters determined for any one compound in a series can be extrapolated to give the parameters for all the others. Values of B_n^m obtained in this way for several other $R\mathrm{Rh_4B_4}$ compounds are also given in Table I.

III. CRYSTALLINE-ELECTRIC-FIELD AND MAGNETIC EFFECTS IN POLYCRYSTALLINE SAMPLES

All paramagnetic susceptibility data previously published have been taken from polycrystalline samples. The general result for these compounds has been that a simple Curie-Weiss law is observed with an effective moment near the free-ion value down to temperatures near the magnetic transitions. This appears to be in conflict with the assumption of relatively large crystal fields in these materials. We have previously discussed this effect and have shown that the observation of simple free-ion-like behavior in the polycrystalline susceptibility should be fairly common in metallic systems where large anisotropies are present, even though the susceptibility obtained in a single crystal may show strong CEF effects.[6] This is illustrated in Fig. 4(a), where the calculated susceptibility for $\mathrm{HoRh_4B_4}$ is given. Parallel to the tetragonal c axis (the easy axis of magnetization for this material), the susceptibility is larger than for the free ion. Although the slope of the inverse susceptibility versus temperature is roughly the same at high temperatures as for the free ion, substantial curvature exists at temperatures below approximately 100 K. Along the a axis (perpendicular to the tetragonal c axis), the susceptibility is much smaller than for the free ion. At high temperatures, the slope is also comparable to that of the free ion, but very strong deviations occur at temperatures below about 50 K. These arise because the CEF ground state in this compound has a small magnetic moment along the a axis, while an excited CEF state has a much larger moment. Also shown in the figure are average susceptibilities formed by weighting the susceptibilities along the a axis (χ_a) and the c axis (χ_c) in varying proportions:

$$\bar{\chi}=n\chi_c+(1-n)\chi_a \ . \tag{6}$$

The value $n=\frac{1}{3}$ corresponds to a random distribution of crystallites relative to H_a for this tetragonal system. From the figure one sees that a randomized sample shows none of the unusual temperature-dependent features, and inspection shows that this gives a Curie-law susceptibility essentially equal to that of the free ion. This feature is common to all the $R\mathrm{Rh_4B_4}$ compounds.

Because of the very large magnetic anistropy, relatively small deviations from a random distribution of crystallites may produce significant curvatures in the temperature dependence of the polycrystalline susceptibilities. Susceptibilities are given in Fig. 4(a) for several values of n,

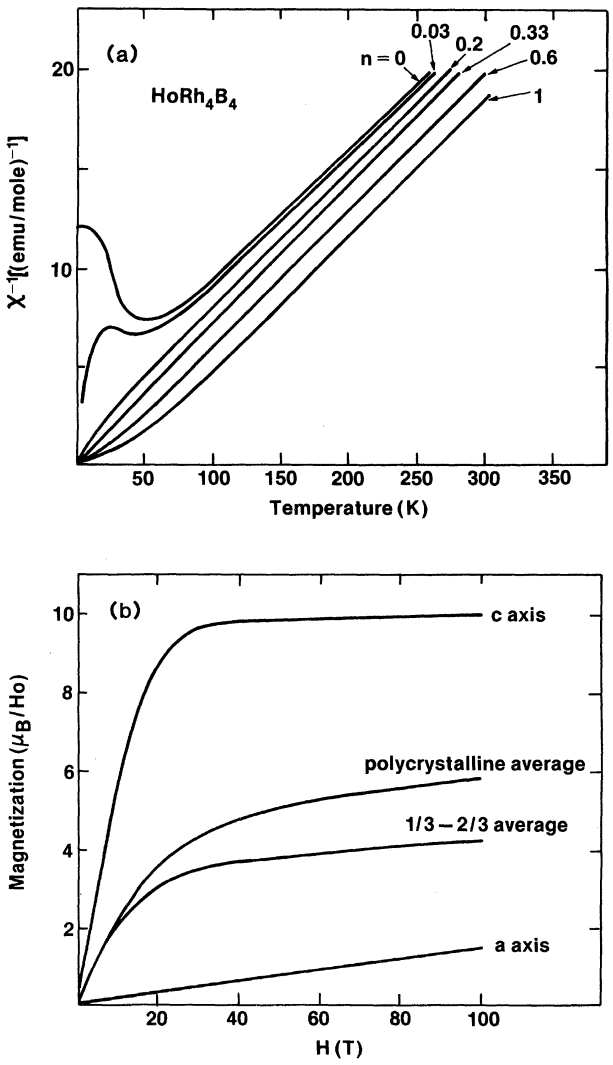

FIG. 4. (a) Calculated susceptibility for $\mathrm{HoRh_4B_4}$ along the c axis ($n=0$), the a axis ($n=1$), a random polycrystalline sample ($n=\frac{1}{3}$), and varying degrees of preferential orientation [see Eq. (3)]. (b) Calculated magnetization for $\mathrm{HoRh_4B_4}$ at $T=10$ K along the a axis, the c axis, and for a polycrystalline sample.

which provides an indication of the deviations that will occur when preferential orientation effects are present.

Figure 4(b) shows the calculated magnetization as a function of applied field at $T=10$ K for $\mathrm{HoRh}_4\mathrm{B}_4$. Here one sees the dramatically large magnetic anisotropy that occurs, with the magnetization varying by 1 order of magnitude between the a and c axes. When the applied field is sufficiently large that M is no longer linear in H_a, the simple averaging procedures of Eq. (6) are no longer valid. The figure shows the polycrystalline magnetization obtained by a numerical integration over angles for each field and temperature assuming a random distribution of crystallite directions relative to H_a, and a comparison with a simple average, $M=\frac{1}{3}M_c+\frac{2}{3}M_a$. In general, the shape of the magnetization curve will depend strongly on the degree of preferential orientation in the material, making detailed comparisons with data very difficult for other than the random case.

In the following we will deal only with phenomena occurring in the paramagnetic state, in order to avoid the complications arising from admixtures of crystal-field levels due to exchange fields. However, in comparing with experimental results it is essential to include exchange effects when magnetic ordering is seen. Because of the temperature dependence introduced in χ by the CEF, it is not appropriate to simply include a Curie-Weiss constant on the temperature scale. Rather, in the mean-field approximation the exchange enhanced susceptibility is given by

$$\frac{1}{\chi}=\frac{1}{\chi_0}-\lambda\ , \tag{7}$$

where χ_0 is the susceptibility from the CEF alone. From Eq. (7) one sees that the mean-field coupling constant λ is related to the magnetic transition temperature T_m according to

$$\lambda=1/\chi_0(T_m)\ , \tag{8}$$

where χ_0 is evaluated along the magnetic easy axis. Although the results discussed above clearly indicate that λ is anisotropic, we presently have no systematic information available. Therefore, in the following we will take λ to be the same in all directions, being determined by the experimental value of T_m through Eq. (8).

IV. COMPARISON WITH POLYCRYSTALLINE EXPERIMENTAL RESULTS

In this section we will compare the available published measurements on magnetization and susceptibility data for the $R\mathrm{Rh}_4\mathrm{B}_4$ compounds with the results of CEF calculations. This includes polycrystalline magnetization and/or susceptibility data for the compounds with $R=$Er, Tm, Ho, and Dy.

A. $\mathrm{ErRh}_4\mathrm{B}_4$

Calculations with the CEF parameters in Table I give the zero-field ground state for the $J=\frac{15}{2}$ manifold of Er^{3+} in $\mathrm{ErRh}_4\mathrm{B}_4$ as

$$0.665\,|\,\pm\tfrac{3}{2}\rangle+0.745\,|\,\mp\tfrac{5}{2}\rangle\ , \tag{9}$$

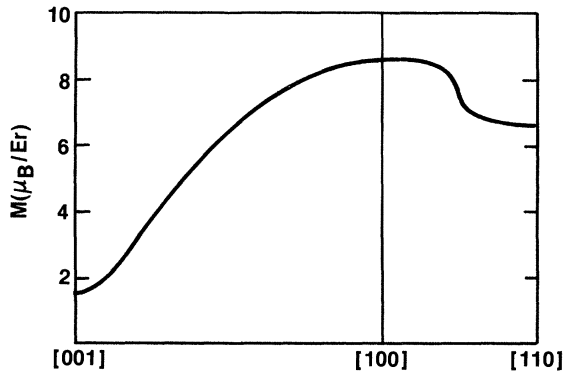

FIG. 5. Angular dependence of the magnetization of $\mathrm{ErRh}_4\mathrm{B}_4$ for $T=2$ K and $H_a=2$ T.

with a first excited state given by

$$0.720\,|\,\pm\tfrac{7}{2}\rangle+0.610\,|\,\mp\tfrac{1}{2}\rangle+0.329\,|\,\mp\tfrac{9}{2}\rangle\ , \tag{10}$$

lying 1.3 K above the ground state.[7] This is in agreement with the magnetic entropy measurements which require four levels lying near one another. With $H_a=0$, these wave functions both give intrinsic values for the magnetic moment along the c axis of about $1\mu_B$, and moments of roughly $3.5\mu_B$ along the a axis. This clearly shows that the basal plane contains the easy axis of magnetization, in agreement with experiment.[8] This becomes more pronounced in the presence of a magnetic field applied along the a axis. Then the wave functions given above are strongly admixed, and the magnetic moment of the ground state rapidly increases. Calculations of the magnetic properties therefore cannot simply make use of the $H_a=0$ wave functions. Figure 5 shows the calculated magnetization in a field applied at various directions relative to the crystalline axes, and provides a summary of ef-

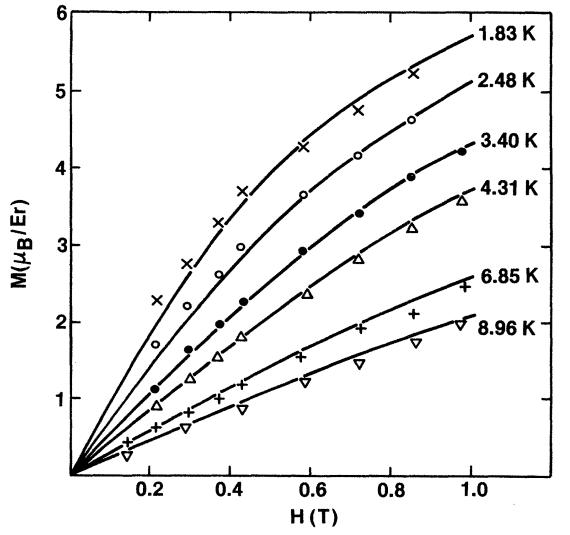

FIG. 6. Magnetization data (Ref. 9) for polycrystalline $\mathrm{ErRh}_4\mathrm{B}_4$. Solid lines are calculated using a full numerical polycrystalline average, assuming a randomized sample.

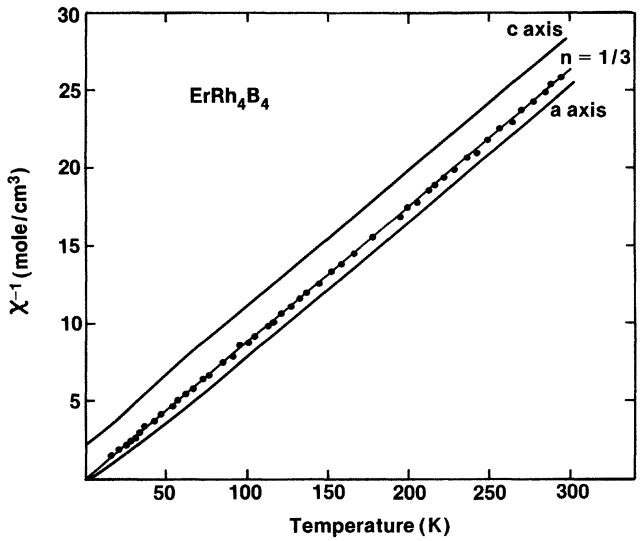

FIG. 7. Measured susceptibility for $ErRh_4B_4$ (solid points, see Ref. 9) and calculated susceptibilities for single-crystal and random polycrystalline samples.

fects seen in the magnetization data discussed above. The principal features of the anisotropic magnetization are saturation magnetization values of $1.6\mu_B$ along the c axis, $8.6\mu_B$ along the a axis, and $6.6\mu_B$ in the [110] direction.

In view of Fig. 5, it is clear that some care must be taken in discussing magnetization data for polycrystalline samples. Magnetization results for polycrystalline $ErRh_4B_4$ are shown in Fig. 6 for the temperature range of 1.83—8.96 K, and applied fields up to 10 kOe.[9] The solid lines in the figure show the results of the crystal-field calculation including a numerical integration over the angular dependence of the moment in both the polar and azimuthal directions. A random distribution of crystallites has been assumed for this calculation, and this is seen to be in good agreement with the data. Figure 7 shows polycrystalline susceptibility data[9] in comparison with results calculated from Eq. (6) for $n=\frac{1}{3}$. One sees that the random orientation assumption also allows a proper description of that data.

B. $HoRh_4B_4$

Applying the crystal-field model to the $J=8$ manifold of Ho^{3+} in $HoRh_4B_4$ gives a ground-state doublet of the approximate form $(1/\sqrt{2})[\,|\pm 8\rangle + |\mp 8\rangle]$. This is an intrinsically nonmagnetic state, but application of very small magnetic fields quickly polarizes the levels into the magnetic doublet $|\pm 8\rangle$. The first excited state is a doublet $|\pm 7\rangle$ at 54 K above the ground state. This compound is extremely anisotropic, with a saturation magnetic moment of $10\mu_B$ along the c direction (easy axis). With $H_a=0$, the perpendicular moment vanishes at low temperatures, but application of a field in the basal plane induces a small moment by admixture of higher-lying states. Figure 8 shows the angular dependence of the saturation moment for varying directions of the applied field. The basal-plane anisotropy here is seen to be very

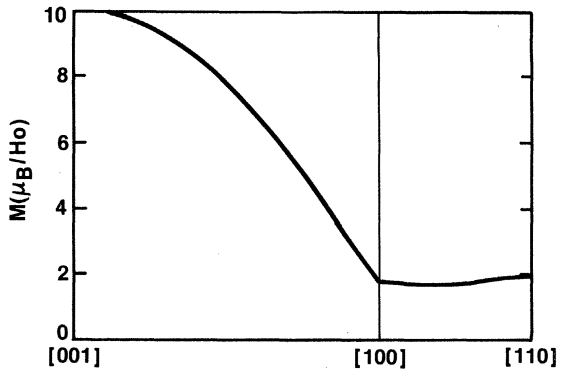

FIG. 8. Angular dependence of the magnetization of $HoRh_4B_4$ for $T=10$ K and $H_a=10$ T.

small, commensurate with the small basal-plane moment. Neutron-diffraction measurements confirm that the c axis is the easy axis of magnetization.[10]

Figure 9 shows the calculated susceptibilities along the c and a axes. This is equivalent to Fig. 4 except that exchange enhancement has been included in both directions appropriate to the magnetic transition temperature of 6.7 K, in accordance with Eqs. (7) and (8). Data exist for two different polycrystalline samples of $HoRh_4B_4$, shown by the closed circles and crosses in Fig. 9.[11,12] In the former, good agreement is obtained with the assumption of random orientation. However, the latter shows distinct curvature in the susceptibility, indicating a nonrandom distribution of crystallites preferentially oriented along the a axis. As seen in the figure, good agreement is obtained with the data using Eq. (6) with a value of $n=0.17$. For this latter sample, high-field magnetization data are also available at a temperature of 10.7 K, shown in Fig. 10.[12] The solid line in the figure shows the calculated magnetization for a random distribution. This reproduces well

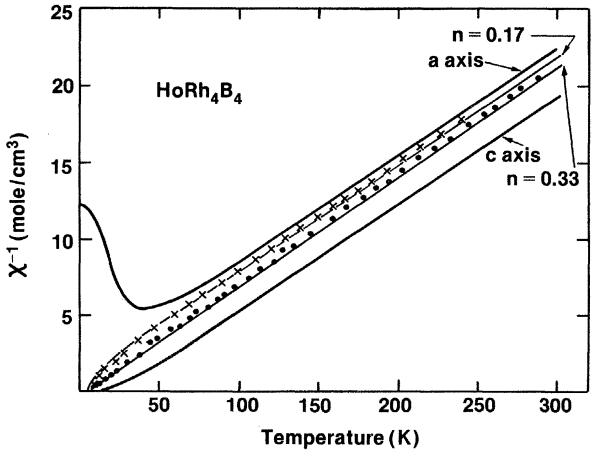

FIG. 9. Measured susceptibilities of polycrystalline $HoRh_4B_4$ from Ref. 11 (●) and Ref. 12 (×). Solid lines show calculated susceptibilities for various degrees of preferential orientation [see Eq. (3)].

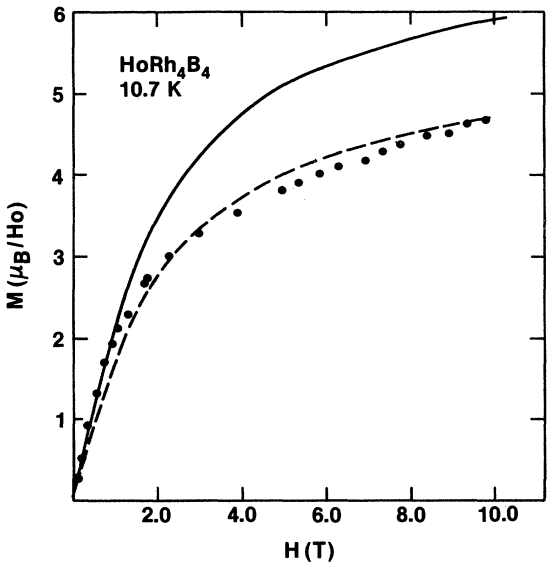

FIG. 10. Measured magnetization for $HoRh_4B_4$ at 10.7 K (solid points, see Ref. 12). The solid line is calculated by numerical averaging assuming a random orientation of crystallites. The dashed line is obtained by reducing the calculated magnetization by 0.80.

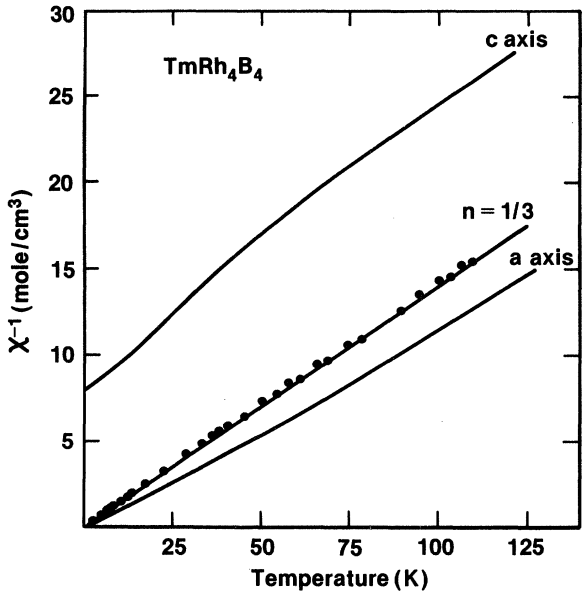

FIG. 11. Measured susceptibility for polycrystalline $TmRh_4B_4$ (closed points, see Ref. 15). Solid lines are calculated for the c axis, a axis, and random polycrystalline orientations.

the field dependence of the data, but the absolute measured values are lower than calculated. This again indicates preferential orientation in the basal plane. No attempt has been made to introduce a detailed model of preferential orientation. The dashed line shows the result of arbitrarily reducing the curve calculated for a random distribution by 0.80.

It should be noted that neutron-diffraction data taken in the ferromagnetic state[10] give a saturation magnetic moment of $8.75\mu_B$, rather than the full value of $10\mu_B$ obtained by this calculation. This may indicate a need to relax the elementary assumption made in obtaining the CEF parameters, whereby a simple scaling through Eq. (5) from the crystal-field parameters of the Er compound has been used. On the other hand, it should also be recalled that there is a discrepancy in the saturation value of the magnetic moment in the ferromagnetic state obtained by neutron diffraction and that found in single-crystal magnetization and in Mössbauer-effect measurements.[4,13] A similar phenomenon may be occurring here, but resolution of this question must await the availability of single crystals of $HoRh_4B_4$.

C. $TmRh_4B_4$

Application of the crystal-field Hamiltonian to the $J=6$ manifold of Tm^{3+} in $TmRh_4B_4$ gives four low-lying levels. The ground state is a nonmagnetic singlet of the form

$$1/\sqrt{2}(|2\rangle+|-2\rangle)\,, \tag{11}$$

the first excited state at 2.6 K above the ground state is a doublet,

$$0.825\,|\pm1\rangle+0.558\,|\mp3\rangle\,, \tag{12}$$

and the third excited state at 5.8 K is a singlet,

$$0.279\,|4\rangle+0.919\,|0\rangle+0.279\,|-4\rangle\,. \tag{13}$$

These are well separated from the higher levels which begin at 31 K. Again, small fields applied in the basal plane cause substantial mixing of the levels, with a large mo-

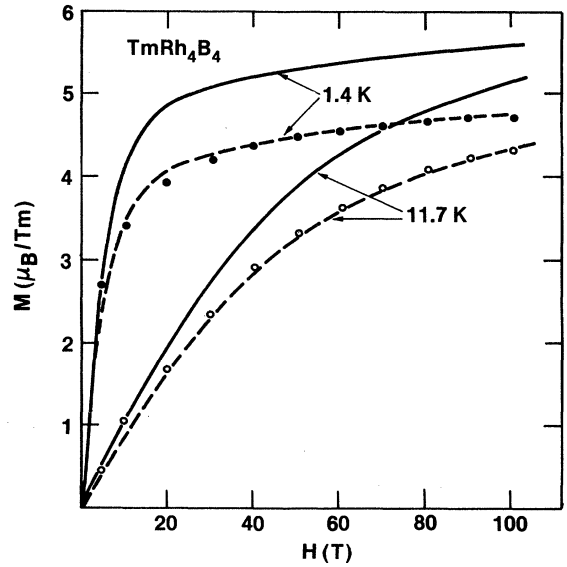

FIG. 12. Measured magnetization (Ref. 16) for $TmRh_4B_4$ at 1.4 K (closed points) and 11.7 K (open points). Solid lines are calculated at those temperatures by numerical integration assuming a random orientation of crystallites. The dashed lines are obtained by reducing the calculated magnetization by 0.85.

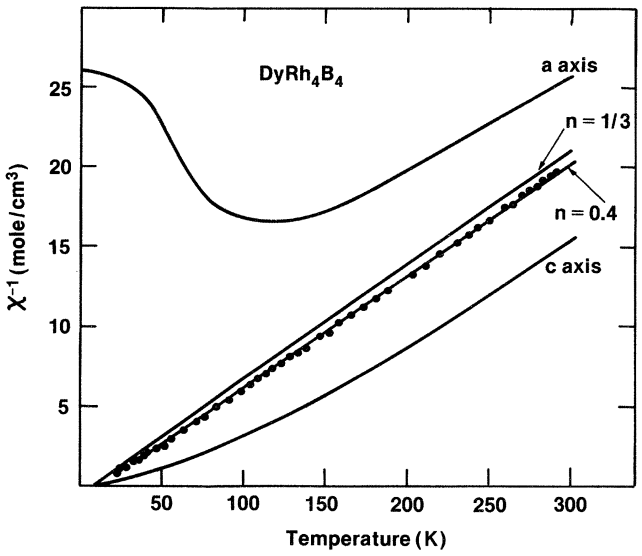

FIG. 13. Measured susceptibility (closed points, Ref. 17) for polycrystalline $DyRh_4B_4$. Solid lines are calculated for the indicated orientations [see Eq. (3)].

ment developing in the basal plane. The angular dependence of the saturation magnetization is very similar to that shown in Fig. 5 for $ErRh_4B_4$, including the extent of the basal-plane anisotropy. Neutron-diffraction measurements verify that the easy axis of magnetization is in the basal plane.[14]

Calculated susceptibilities along the a and c axes for $TmRh_4B_4$ are shown in Fig. 11. Comparison with the experimental data[15] shows good agreement assuming a random distribution of crystallites. High-field magnetization data are also available, shown in Fig. 12.[16] The solid line in the figure shows the results of a polycrystalline average assuming random orientations, and the dashed lines give those results arbitrarily reduced by 0.85, again indicating some preferential orientation toward the hard axis of magnetization for that particular sample.

D. $DyRh_4B_4$

Crystal-field calculations for the $J=\frac{15}{2}$ manifold of the Dy^{3+} ion in $DyRh_4B_4$ give a simple ground-state doublet $|\pm\frac{15}{2}\rangle$ with a $|\pm\frac{13}{2}\rangle$ doublet at 134 K. This results in an extremely anisotropic magnetization with the c axis being the easy axis of magnetization. The angular distribution of the saturation magnetization is very similar to that shown in Fig. 8 for $HoRh_4B_4$. The calculated susceptibilities, including exchange effects due to the magnetic transition at 10.7 K, are shown in Fig. 13. The observed susceptibilities[17] are in good agreement with the calculated values for $n=0.4$, rather than the random orientation value of $\frac{1}{3}$ [see Eq. (6)]. It was previously suggested[17] that the observed deviation from linearity for $1/\chi$ vs T was due to crystal-field effects, however, this is seen to be due to preferential orientation effects. No magnetization data exist for this material.

E. Magnetic transition temperatures

It has been frequently noted that the variation of the magnetic transition temperatures with R in the RRh_4B_4 series does not follow the de Gennes rules, $T_m \sim(g_J-1)^2J(J+1)$, which is expected in the absence of CEF effects. Noakes and Shenoy[18] have shown that much of the discrepancy can be resolved when CEF effects are included. With the use of a simplified Hamiltonian containing only the term in O_2^0, a formal calculation showed that values of T_m could be strongly enhanced when strong magnetic anisotropies are present, and that the peak in the T_m vs R plot occurred with Tb rather than Gd. For a more general CEF Hamiltonian, numerical procedures are most easily used to include the CEF effects. Within the context of a mean-field model, Eq. (8) may be applied and scaled from one rare earth to another according to

$$\lambda=\lambda_0(g_J-1)^2/g_J^2 . \tag{14}$$

By utilizing the measured value of T_m for one compound to determine λ_0, Eqs. (8) and (14) may be coupled with numerical calculations of the susceptibility along the easy axis to obtain the magnetic transition temperature for other members of the series.

It is easily seen that this procedure also provides the enhancement demonstrated by Noakes and Shenoy. For a crystal-field ground state given by $|J_z=\pm J\rangle$, the susceptibility in the easy direction is

$$\chi=\frac{Ng_J^2\mu_B^2J^2}{kT} . \tag{15}$$

With the use of Eqs. (8) and (15), this gives a magnetic transition temperature

$$T_m=\frac{N\lambda_0\mu_B(g_J-1)^2J^2}{k} \tag{16}$$

compared to the value in the absence of crystal fields given by

$$T_m^0=\frac{N\lambda_0\mu_B(g_J-1)^2J(J+1)}{3k} . \tag{17}$$

The enhancement $T_m/T_m^0=3J/(J+1)$ is the same as that which was obtained by Noakes and Shenoy.

Figure 14 shows the results obtained by this procedure using the measured $T_m=5.8$ K for $GdRh_4B_4$ to determine λ_0. Susceptibilities were calculated using the full crystal-field Hamiltonian for the appropriate easy direction (the a axis for Er, Tm, and Sm, and the c axis for the remainder). It should be emphasized that a procedure such as this is appropriate only for ferromagnetic compounds since it utilizes only the static susceptibility. However, for completeness, the calculation has been carried out for all the materials, with the measured antiferromagnetic compounds being noted in the figure.

From the figure, one sees that little is changed from Ref. 18 by the inclusion of the additional CEF terms. In particular, the calculation still gives a peak of T_m at Tb, while the experimental values peak at Dy. In general, there remain discrepancies in the calculated values of 1–3 K. In order to fully understand these results, it will there-

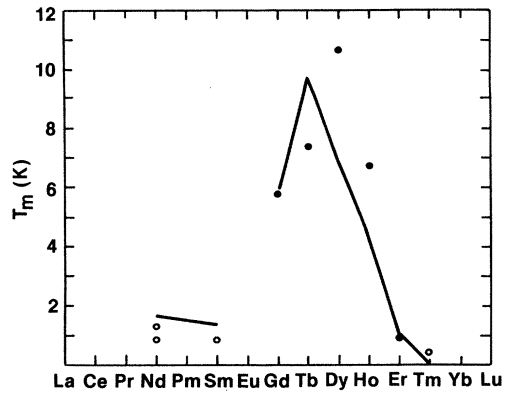

FIG. 14. Measured magnetic transition temperatures for $R\mathrm{Rh}_4\mathrm{B}_4$ compounds showing both ferromagnetic (closed points) and antiferromagnetic (open points) transitions. Solid line is calculated as described in the text.

fore be necessary to include other mechanisms, the most obvious being the influence of dipolar interactions and the possibility of anisotropic exchange.

V. CONCLUSIONS

A detailed analysis has been given for the magnetic properties of the $R\mathrm{Rh}_4\mathrm{B}_4$ materials within a combined crystal-field and molecular-field model. This has provided improved values for crystal-field coefficients over those previously presented. The current parameters adequately describe the field and temperature dependence of the paramagnetic magnetization of single-crystal $\mathrm{ErRh}_4\mathrm{B}_4$ in five different orientations. In addition, all previously published polycrystalline magnetization and susceptibility data for various $R\mathrm{Rh}_4\mathrm{B}_4$ compounds have been described, and the effects of preferential crystallite orientation on the magnetic measurements have been pointed out. Application of the crystal-field model to the R dependence of the magnetic transition temperature has verified a previous conclusion that the CEF has an important effect on T_m, but does not completely explain the observations.

ACKNOWLEDGMENTS

This work was supported by Office of Basic Energy Sciences, Division of Materials Sciences, the U.S. Department of Energy under Contract No. W-7405-Eng-82.

[1]For a review of the properties of these materials, see M. B. Maple, H. C. Hamaker, and L. D. Woolf, in *Superconductivity in Ternary Compounds II,* Vol. 34 of *Topics in Current Physics,* edited by M. B. Maple and Ø. Fischer (Springer, Berlin, 1982), pp. 99–142.

[2]B. D. Dunlap and D. Niarchos, Solid State Commun. 44, 1577 (1982).

[3]H. B. Radousky, B. D. Dunlap, G. S. Knapp, and D. G. Niarchos, Phys. Rev. B 27, 5526 (1983).

[4]G. W. Crabtree, F. Behroozi, S. A. Campbell, and D. G. Hinks, Phys. Rev. Lett. 49, 1342 (1982).

[5]L. N. Hall, F. Behroozi, S. A. Campbell, G. W. Crabtree, and D. G. Hinks, Bull. Am. Phys. Soc. 28, 281 (1983).

[6]B. D. Dunlap, J. Magn. Magn. Mater. 37, 211 (1983).

[7]Eigenstates are given in terms of pure angular momentum states $|J_z\rangle$, with z along the tetragonal c axis.

[8]D. E. Moncton, D. B. McWhan, J. Eckert, G. Shirane, and W. Thomlinson, Phys. Rev. Lett. 39, 1164 (1977).

[9]W. A. Fertig, D. C. Johnston, L. E. DeLong, R. W. McCallum, M. B. Maple, and B. T. Matthias, Phys. Rev. Lett. 38, 987 (1977); D. C. Johnston (private communication).

[10]G. H. Lander, S. K. Sinha, and F. Y. Fradin, J. Appl. Phys. 50, 1990 (1979); H. A. Mook, W. C. Koehler, M. B. Maple, Z. Fisk, D. C. Johnston, and L. D. Woolf, Phys. Rev. B 25, 372 (1982).

[11]M. B. Maple, H. C. Hamaker, D. C. Johnston, H. B. MacKay, and L. D. Woolf, J. Less-Common Met. 52, 251 (1978).

[12]H. R. Ott, L. D. Woolf, M. B. Maple, and D. C. Johnston, J. Low Temp. Phys. 39, 383 (1980).

[13]G. K. Shenoy, B. D. Dunlap, F. Y. Fradin, S. K. Sinha, C. W. Kimball, W. Potzel, F. Pröbst, and G. M. Kalvius, Phys. Rev. B 9, 3886 (1980).

[14]C. F. Majkrzak, S. K. Satija, G. Shirane, H. C. Hamaker, Z. Fisk, and M. B. Maple, Phys. Rev. B 27, 2889 (1983).

[15]H. C. Hamaker, M. B. MacKay, L. D. Woolf, M. B. Maple, W. Odoni, and H. R. Ott, Phys. Lett. 81A, 91 (1981).

[16]H. R. Ott, H. Rudigier, H. C. Hamaker, and M. B. Maple, in *Ternary Superconductors,* edited by G. K. Shenoy, B. D. Dunlap, and F. Y. Fradin (North-Holland, New York, 1981), pp. 159–162.

[17]H. B. MacKay, L. D. Woolf, M. B. Maple, and D. C. Johnston, J. Low Temp. Phys. 41, 639 (1980).

[18]D. R. Noakes and G. K. Shenoy, Phys. Lett. 91A, 35 (1982).

[19]P. Fulde, in *Physics and Chemistry of Rare-Earths,* edited by K. A. Gschneidner, Jr., and L. Eyring (North-Holland, Amsterdam, 1970), p. 300.